WAR Journal of Multidisciplinary Bulletin
(WARJMB)

ISSN (Online): 1595-6709
ISSN (Print): 1595-6636

Received: 02-10-2025 Revised: 26-10-2025 Accepted: 05-11-2025 Published: 18-11-2025

Research Article

RESEARCH ON TRAJECTORY TRACKING CONTROL METHOD OF AGV USING ACTIVE DISTURBANCE REJECTION CONTROLLER

Hyang Sim Pak[1], Se Yang Pak[2], Chol Jun Han[3], *

[1]Robotics Institute, Kim Chaek University of Technology, Pyongyang, Democratic People's Republic of Korea

[2]Faculty of Automatics, Kim Chaek University of Technology, Pyongyang, Democratic People's Republic of Korea

[3]Robotics Institute, Kim Chaek University of Technology, Pyongyang, Democratic People's Republic of Korea

.

OPEN ACCESS

Published in
VOI- 1 Issue: 5

DOI:10.5281/zenodo.17680943

PP: 01-17

***Correspondence:**

Chol Jun Han

RoboticsInstitute, Kim Chaek University of Technology, Pyongyang, Democratic People's Republic of Korea
Email: rus89115@star-co.net.kp

Abstract

In this paper, discrete time active disturbance rejection control (ADRC) method based on a novel variable pole placement extended state observer (VPPESO) is presented for trajectory tracking of automated guided vehicle (AGV) driven by two wheels. If the road is not smooth or the loading weight of the AGV is varied, the friction resistance of the wheels and the load torque of the motor will fluctuate, which will act as disturbance to the control system. The control system has a cascade control structure containing an external loop and an internal loop. The outer control loop determines the desired moving speed and steering angle as the set point of the inner control loop based on the target trajectory the current position and velocity of AGV. The inner control loop realizes active disturbance rejection control (ADRC) based on the dynamic model of AGV. The effectiveness of the control system is verified via simulation.

Keywords: AGV; VPPESO; trajectory tracking control; ADRC.

Introduction

Automated guided vehicles (AGVs) are a kind of unmanned robots, which are widely used in many fields, including military, economic and agricultural applications [1-3]. Generally, AGVs consist of actuators, sensors and control systems, and commonly used sensors are laser sensors, ultrasonic sensors, GPS, etc. and the actuator is determined by the running driving mode.

The control system determines the overall performance of AGV. Generally, AGV must have the function of trajectory tracking for performing the task. A two wheel driving AGV based on differential steering is the imperfect driving system which has three degrees of freedom and two control inputs. Therefore, it is a difficult task to realize the precise trajectory tracking of AGV with model uncertainties, nonlinearities and disturbances. In general, PID control, sliding mode control (SMC), and optimal control

Copyright © 2025, Authors retain copyright. Licensed under the Creative Commons Attribution 4.0 International License (CC BY 4.0), which permits unrestricted use, distribution, and reproduction in any medium, provided the original work is properly cited. https://creativecommons.org/licenses/by/4.0/ (CC BY 4.0 deed)

WAR Journal of Multidisciplinary Bulletin
(WARJMB)
ISSN (Online): 1595-6709
ISSN (Print): 1595-6636
Received: 02-10-2025 Revised: 26-10-2025 Accepted: 05-11-2025 Published: 18-11-2025

methods are used in the tracking control of AGVs [4-5]. In [6], a sliding mode control approach was given to facilitate fast convergence and strong robustness, and was combined with fuzzy systems to reduce the oscillation. An improved method was proposed to develop an integrated control strategy for path tracking and lateral motion stabilization of autonomous distributed electric vehicles [7]. The second-order sliding mode control of the super twisting algorithm was proposed for an experimental car-like system called the Robucar to vanish asymptotically tracking errors [8]. The sliding mode control method has good robustness on the uncertainty of the system parameters and external disturbances. ADRC is a state feedback control system that uses an extended state observer to estimate the unknown disturbances acting on the system and improves the control performance by compensating the estimated disturbances. Although active disturbance rejection control can be designed for both continuous time and discrete time systems, most of the previous have been designed for continuous time systems because the dynamics of AGV systems are derived from continuous models [9-11]. In [12], an improved ADRC is proposed for the design of a robust trajectory tracking control of a fully actuated unmanned surface vessel in the presence of complex time varying disturbances; parameters uncertainties; and sensors noise.

In [13], was proposed an advanced robust active disturbance rejection control (ADRC) for flexible link manipulator (FLM) to track desired trajectories in the joint space and minimize the link's vibrations. In [14], we apply the active disturbance rejection control approach to output feedback stabilization for uncertain lower triangular nonlinear systems with stochastic inverse dynamics and stochastic disturbance.

In [15-16], they designed the discrete ESO with variable gain to improve the transient performance of ADRC and proved the stability of state estimation error and control error.

We overcome the problems of previous works by constructing an extended state observer using the variable pole placement method to improve the accuracy of trajectory tracking. The description of the paper is organized as follows.

Section 2 describes the configuration of the tracking system and the outer loop control system.

Section 3 describes the design of an ESO based on the variable pole placement.

In Section 4, the tracking performance of AGV using the variable pole placement method and the estimation accuracy of observer are verified via simulation.

Construction of trajectory tracking control system

The trajectory tracking control system of AGV consists of a cascade control system with dual loop control as shown in Figure 1. The outer loop realizes the control of the moving trajectory and the inner loop realizes the control of the AGV's travel speed and direction of motion (attitude). The outer loop controller provides the reference velocity and attitude angle for the inner control loop based on the trajectory tracking error.

Copyright © 2025, Authors retain copyright. Licensed under the Creative Commons Attribution 4.0 International License (CC BY 4.0), which permits unrestricted use, distribution, and reproduction in any medium, provided the original work is properly cited. https://creativecommons.org/licenses/by/4.0/ (CC BY 4.0 deed)

WAR Journal of Multidisciplinary Bulletin
(WARJMB)
ISSN (Online): 1595-6709
ISSN (Print): 1595-6636
Received: 02-10-2025 Revised: 26-10-2025 Accepted: 05-11-2025 Published: 18-11-2025

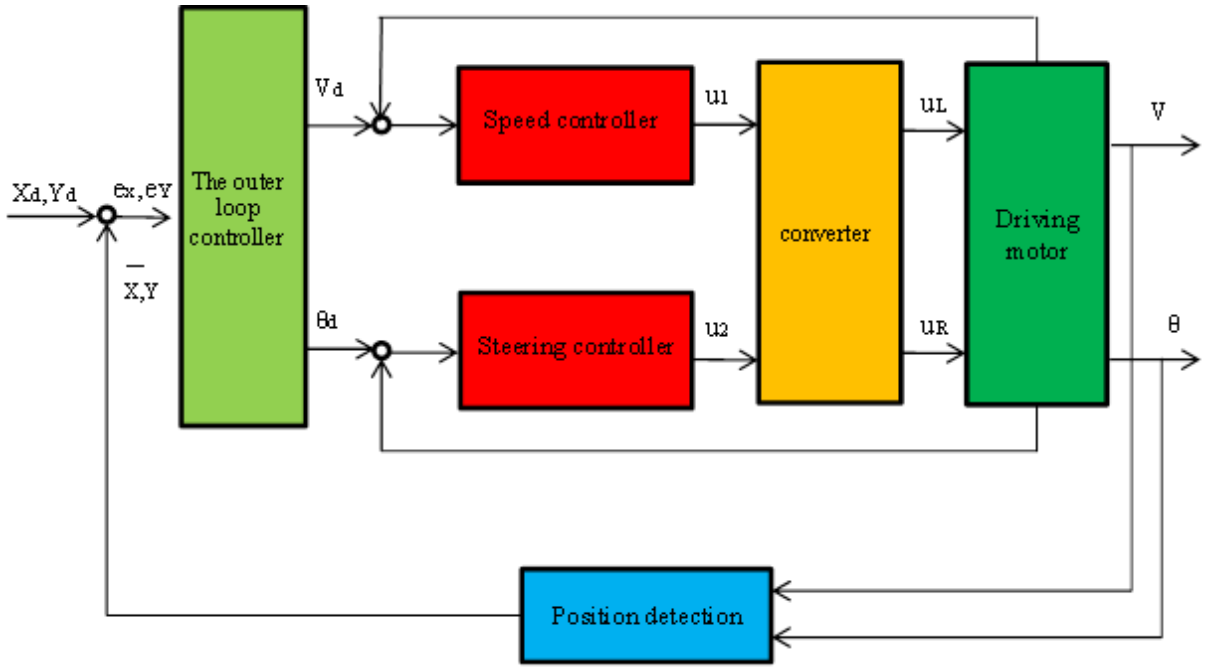

Figure 1. Trajectory tracking control structure of AGV.

The position coordinates of AGV are denoted by (X, Y). The kinematic equation of AGV for tracking the trajectory can be modeled as follows:

$$\dot{X} = v\cos\theta \quad (1)$$

$$\dot{Y} = v\sin\theta \quad (2)$$

Let $[X_{d(t)}, Y_{d(t)}]$ be the desired trajectory and $[e_X, e_Y]$ be the tracking error , the error dynamics is given as:

$$\dot{e}_X = v\cos\theta - \dot{X}_d \quad (3)$$

$$\dot{e}_Y = v\sin\theta - \dot{Y}_d \quad (4)$$

By defining $u_1 = v\cos\theta, u_2 = v\sin\theta$ and taking the control input as

$$u_1 = \dot{X}_d - k_1 e_x \quad (5)$$

$$u_2 = \dot{Y}_d - k_2 e_Y \quad (6)$$

the error dynamics are represented as follows.

$$\dot{e}_x = -k_1 e_x \quad (7)$$

$$\dot{e}_Y = -k_2 e_Y \quad 8)$$

where $k_1 > 0, k_2 > 0$.

Thus, defining two Lyapunov functions as

$$V_X = \frac{1}{2} e_X^2 \quad (9)$$

$$V_Y = \frac{1}{2} e_Y^2 \quad (10)$$

Copyright © 2025, Authors retain copyright. Licensed under the Creative Commons Attribution 4.0 International License (CC BY 4.0), which permits unrestricted use, distribution, and reproduction in any medium, provided the original work is properly cited. https://creativecommons.org/licenses/by/4.0/ (CC BY 4.0 deed)

WAR Journal of Multidisciplinary Bulletin
(WARJMB)
ISSN (Online): 1595-6709
ISSN (Print): 1595-6636
Received: 02-10-2025 Revised: 26-10-2025 Accepted: 05-11-2025 Published: 18-11-2025

yields

$$\dot{V}_X = e_X \dot{e}_X = -k_1 e_X^2 = -2k_1 V_X \le 0 \quad (11)$$

$$\dot{V}_Y = e_Y \dot{e}_Y = -k_2 e_Y^2 = -2k_2 V_Y \le 0 \quad (12)$$

This means that the system is stable.

From the control laws Eq. (5) and Eq. (6), θ_d and V_d to be required for the AGV to track the desired trajectory are obtained as follows:

$$\theta_d = \arctan \frac{u_2}{u_1} \quad (13)$$

$$v_d = \begin{cases} \sqrt{u_1^2 + u_2^2} & -\frac{\pi}{2} < e_\theta < \frac{\pi}{2} \\ 0 & e_\theta = \pm \frac{\pi}{2} \\ -\sqrt{u_1^2 + u_2^2} & \end{cases} \quad (14)$$

Where, eθ is the error between the desired attitude angle and the actual one.

$$e_\theta = \theta_d - \theta$$

Design of discrete active disturbance rejection controller

Here we design the inner control loop system for the steering angle and speed to approach the reference values obtained from the outer control loop. In the inner control loop system, the voltage of the two driving wheels is controlled to achieve the control of the steering angle and velocity.

Dynamics model of AGV

The dynamic of the two-wheel AGV is shown in Figure 2.

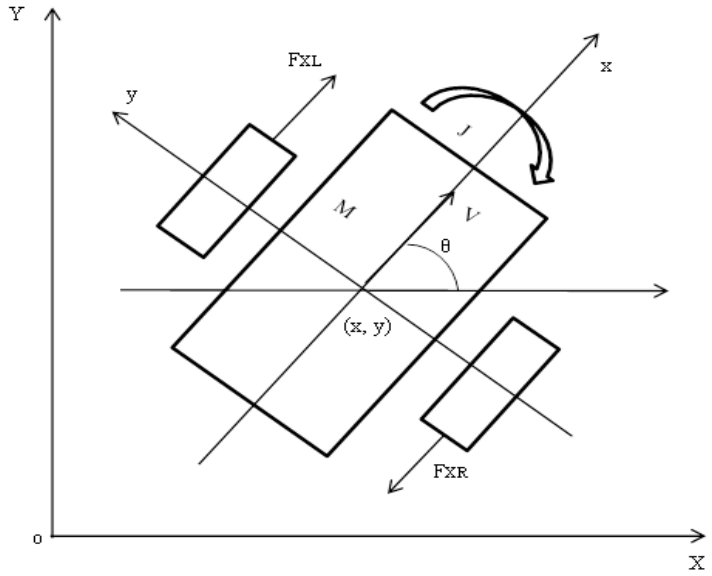

Figure 2. Coordinate of AGV.

Copyright © 2025, Authors retain copyright. Licensed under the Creative Commons Attribution 4.0 International License (CC BY 4.0), which permits unrestricted use, distribution, and reproduction in any medium, provided the original work is properly cited. https://creativecommons.org/licenses/by/4.0/ (CC BY 4.0 deed)

WAR Journal of Multidisciplinary Bulletin
(WARJMB)
ISSN (Online): 1595-6709
ISSN (Print): 1595-6636
Received: 02-10-2025 Revised: 26-10-2025 Accepted: 05-11-2025 Published: 18-11-2025

According to Newton's law, the moment balance equations of the left and right wheels are described as follows:

$$T_L - T_{zL} = J\frac{d\omega L}{dt} \quad (15)$$

$$T_R - T_{zR} = J\frac{d\omega R}{dt} \quad (16)$$

Where TL and TR denote electromagnetic torque of left and right motors and TZL and TZR denote the load torque of left and right motors, respectively. Since the motor load torque is produced by the friction force that impedes the rotational motion of the wheel, Eq. (15) and Eq. (16) can be written as:

$$T_L = T_{zL} + J\frac{d\omega_L}{dt} = f_L r + J\frac{d\omega_L}{dt} \quad (17)$$

$$T_R = T_{zR} + J\frac{d\omega_R}{dt} = f_R r + J\frac{d\omega_R}{dt} \quad (18)$$

where f_L and f_R denote the friction forces acting on the left and right wheels, and r denote the radius of the wheel. Eq. (17) and Eq. (18) are expressed in terms of forces as follows:

$$f_L - F_{xL} = m\frac{dv_L}{dt} = mr\dot{\omega}_L \quad (19)$$

$$f_R - F_{xR} = m\frac{dv_R}{dt} = mr\dot{\omega}_R \quad (20)$$

where, F_{xL} and F_{xR} denote the forces in the x-direction acting on the left and right wheels, respectively. If their reaction forces are represented as F'_{xL} and F'_{xR}, respectively, according to Newton's third law, which found that the action and reaction are equal in magnitude and opposite in direction, and are expressed as follows :

Therefore $F_{xL} = -F'_{xL}$, $F_{xR} = -F'_{xR}$.

Hence, the dynamic equation for the velocity and the direction angle of the AGV body is expressed as follows:

$$F'_{xL} + F'_{xR} - f_L - f_R = M\dot{v} = M(\dot{\omega}_L + \dot{\omega}_R)r/2 \quad (21)$$

$$(F'_{xR} - F'_{xL}) \cdot l/2 = Jz\ddot{\theta} = Jz(\dot{\omega}_R - \dot{\omega}_L)r/l \quad (22)$$

where, V is the velocity, M is the mass, Jz is the moment of inertia, and θ is the steering angle of the body Now, if we ignore the friction force and use the definitions of $u_1 = F'_{XL} + F'_{XR}$ and $u_2 = F'_{XL} - F'_{XR}$, we have

Copyright © 2025, Authors retain copyright. Licensed under the Creative Commons Attribution 4.0 International License (CC BY 4.0), which permits unrestricted use, distribution, and reproduction in any medium, provided the original work is properly cited. https://creativecommons.org/licenses/by/4.0/ (CC BY 4.0 deed)

WAR Journal of Multidisciplinary Bulletin
(WARJMB)
ISSN (Online): 1595-6709
ISSN (Print): 1595-6636
Received: 02-10-2025 Revised: 26-10-2025 Accepted: 05-11-2025 Published: 18-11-2025

$$M\dot{v} = u_1 \quad (23)$$

$$J\ddot{\theta} = u_2 \quad (24)$$

Expressing the dynamic models of Eq. (23) and Eq. (24) as the transfer functions, the velocity control and steering control plants are respectively expressed as follows:

$$G_1(s) = \frac{k_1}{s} \quad (25)$$

$$G_2(s) = \frac{k_2}{s^2} \quad (26)$$

Since Eq. (25) is an integral component, it can be stabilized enough by proportional feedback. Therefore, the speed control loop is constructed by a proportional feedback controller and the detailed controller coefficients are determined through simulation and experiment. Since the steering dynamics model of Eq. (26) is a second order integral system and is actually affected by model uncertainties and disturbances, it is necessary to apply a more effective control method to effectively suppress disturbances.

Design of ADRC

Here we design the ADRC system by using an ESO with variable poles for the steering angle control.

Discrete state space model of control plant

For the extended state observer design, we first converse the steering angular dynamics model expressed by Eq. (26), to a state space model. At this time, the state vector is expanded by including the disturbance torque applied to the system as a new state variable.

That is, when the state vector is denoted as x, the state space model of the control plant can be expressed as:

$$\begin{aligned} \dot{x}(t) &= Ax(t) + Bu(t) + E\omega(t) \\ y(t) &= Cx(t) \end{aligned} \quad (27)$$

Where

$$A = \begin{bmatrix} 0 & 1 & 0 \\ 0 & 0 & 1 \\ 0 & 0 & 0 \end{bmatrix}, \mathrm{B} = \begin{bmatrix} 0 & b & 0 \end{bmatrix}^T, \mathrm{C} = \begin{bmatrix} 1 & 0 & 0 \end{bmatrix}^T \quad (28)$$

$$\mathrm{E} = \begin{bmatrix} 0 & 0 & 1 \end{bmatrix}^T, b = \frac{\ell}{2Jz}$$

The discrete state space model is obtained by discretizing Eq. (27) as follows:

$$\begin{aligned} x(k+1) &= \Phi x(k) + \Gamma_u u(k) + Eh(k), \\ y(k) &= Hx(k) \end{aligned} \quad (29)$$

Copyright © 2025, Authors retain copyright. Licensed under the Creative Commons Attribution 4.0 International License (CC BY 4.0), which permits unrestricted use, distribution, and reproduction in any medium, provided the original work is properly cited. https://creativecommons.org/licenses/by/4.0/ (CC BY 4.0 deed)

WAR Journal of Multidisciplinary Bulletin
(WARJMB)
ISSN (Online): 1595-6709
ISSN (Print): 1595-6636
Received: 02-10-2025 Revised: 26-10-2025 Accepted: 05-11-2025 Published: 18-11-2025

Where

$$\Phi = \begin{bmatrix} 1 & T & \frac{T^2}{2} \\ 0 & 1 & T \\ 0 & 0 & 1 \end{bmatrix}, \Gamma_u = \begin{bmatrix} \frac{b_1 T^2}{2} & b_1 T & 0 \end{bmatrix}^T$$

, and T is the sampling period.

$$, h(k) = \int_0^T e^{A\tau} E\omega((k+1)T - \tau)d\tau, H = \begin{bmatrix} 1 & 0 & 0 \end{bmatrix}$$

Discrete variable pole placement extended state observer (VPPESO)

The discrete extended state observer for the control plant, Eq. (29) is expressed as:

$$\hat{x}(k+1) = \Phi\hat{x}(k) + \Gamma_u u(k) + L(e_1(k))(y(k) - \hat{y}(k)),$$
$$\hat{y}(k) = H\hat{x}(k) \qquad (30)$$

Where

$$\hat{x} = \begin{bmatrix} \hat{x}_1(k) & \hat{x}_2(k) & \hat{x}_3(k) \end{bmatrix}^T, e_1(k) =$$
$$= x_1(k) - \hat{x}_1(k), L(e_1(k))$$
$$= \begin{bmatrix} \ell_1(e_1(k)) & \ell_2(e_1(k)) & \ell_3(e_1(k)) \end{bmatrix}^T$$

In the VPPESO, the observer feedback gain is adaptively modified based on the state estimation error to fully estimate the unknown disturbances varied over a relatively wide range.

The dynamic equation for the estimation error of the state observer is expressed as:

$$e(k+1) = \bar{A}(k)e(k) + Bh(k) \qquad (31)$$

Where

$e(k) = x(k) - \hat{x}(k)$ and the system matrix $\bar{A}(k)$ is expressed as:

$$\bar{A}(k) = \Phi - L(e_1(k))H =$$
$$\begin{bmatrix} 1 & T & \frac{T^2}{2} \\ 0 & 1 & T \\ 0 & 0 & 1 \end{bmatrix} - \begin{bmatrix} \ell_1(e_1(k)) \\ \ell_2(e_1(k)) \\ \ell_3(e_1(k)) \end{bmatrix} \begin{bmatrix} 1 & 0 & 0 \end{bmatrix} = \qquad (32)$$
$$\begin{bmatrix} 1 - \ell_1(e_1(k)) & T & \frac{T^2}{2} \\ -\ell_2(e_1(k)) & 1 & T \\ -\ell_3(e_1(k)) & 0 & 1 \end{bmatrix}$$

Copyright © 2025, Authors retain copyright. Licensed under the Creative Commons Attribution 4.0 International License (CC BY 4.0), which permits unrestricted use, distribution, and reproduction in any medium, provided the original work is properly cited. https://creativecommons.org/licenses/by/4.0/ (CC BY 4.0 deed)

WAR Journal of Multidisciplinary Bulletin
(WARJMB)
ISSN (Online): 1595-6709
ISSN (Print): 1595-6636
Received: 02-10-2025 Revised: 26-10-2025 Accepted: 05-11-2025 Published: 18-11-2025

Since the performance of the state estimation of the ESO is determined by the root of the characteristic equation, i.e., the location of the poles, the characteristic equation is expressed as:

$$\det|\lambda I - \bar{A}| = \begin{bmatrix} \lambda - 1 + \ell_1(e_1(k)) & -T & -\frac{T^2}{2} \\ \ell_2(e_1(k)) & \lambda - 1 & -T \\ \ell_3(e_1(k)) & 0 & \lambda - 1 \end{bmatrix} =$$

$$= (\lambda - 1)^2(\lambda - 1 + \ell_1(e_1(k))) + T^2\ell_3(e_1(k)) +$$

$$(\lambda - 1)\frac{T^2}{2}c\ell_3(e_1(k)) + (\lambda - 1)T\ell_2(e_1(k)) = \quad (33)$$

$$= (\lambda - 1)^3 + \ell_1(e_1(k))(\lambda - 1)^2 + (\frac{T^2}{2}\ell_3(e_1(k))$$

$$+ T\ell_2(e_1(k)))(\lambda - 1) + T^2\ell_3(e_1(k)) = 0$$

This is a third order polynomial with respect to (λ-1).

Denoting the desired poles of the observer by P1, P2, and P3, the characteristic equation can be written as

$$(\lambda - P_1)(\lambda - P_2)(\lambda - P_3) = \lambda^3 - (P_1 + P_2 + P_3)\lambda^2$$
$$+ (P_1P_2 + P_2P_3 + P_1P_3)\lambda - P_1P_2P_3 = 0 \quad (34)$$

Comparing two equations Eq. (33) and Eq. (34), the equations between the coefficients of two polynomials are expressed as:

$$\begin{cases} \ell_1(e_1(k)) = -(P_1 + P_2 + P_3) \\ \frac{T^2}{2}\ell_3(e_1(k)) + T\ell_2(e_1(k)) = P_1P_2 + P_2P_3 + P_1P_3 \\ T^2\ell_3(e_1(k)) = -P_1P_2P_3 \end{cases} \quad (35)$$

From Eq. (35), the formula for determining the observer gain corresponding to the desired poles is obtained as follows:

$$L(e_1(k)) = \begin{bmatrix} \ell_1(e_1(k)) \\ \ell_2(e_1(k)) \\ \ell_3(e_1(k)) \end{bmatrix} =$$

$$\begin{bmatrix} -(P_1' + P_2' + P_3') \\ \frac{1}{T}(P_1'P_2' + P_2'P_3' + P_1'P_3' + \frac{1}{2}P_1'P_2'P_3') \\ -\frac{1}{T^2}P_1'P_2'P_3' \end{bmatrix} \quad (36)$$

where $P_i' = P_i - 1, i = 1,2,3$.

Copyright © 2025, Authors retain copyright. Licensed under the Creative Commons Attribution 4.0 International License (CC BY 4.0), which permits unrestricted use, distribution, and reproduction in any medium, provided the original work is properly cited. https://creativecommons.org/licenses/by/4.0/ (CC BY 4.0 deed)

WAR Journal of Multidisciplinary Bulletin
(WARJMB)
ISSN (Online): 1595-6709
ISSN (Print): 1595-6636
Received: 02-10-2025 Revised: 26-10-2025 Accepted: 05-11-2025 Published: 18-11-2025

The poles of the ESO are chosen as a function of the error e(k) so that the location of the poles is varied by the magnitude of state estimation error adaptively.

Feedback controller design

ADRC is a control method that can reject effectively the disturbance. This method represents the unknown disturbance acting on the system and the un-modeled uncertain dynamics as equivalent extended disturbances and estimates them by using an ESO. First, the state feedback manipulated variable u0 is determined by linear quadratic LQ optimal control to stabilize the system. In the case of disturbances and model uncertainties, the state equations of the controlled plant are expressed as:

$$x(k+1) = \Phi_0 x(k) + \Gamma_0 u(k)$$
$$y(k) = H_0 x(k) \qquad (38)$$

where

$$\Phi_0 = \begin{bmatrix} 1 & T \\ 0 & 1 \end{bmatrix}, \Gamma_0 = \begin{bmatrix} 0 & bT \end{bmatrix}^T, H_0 = \begin{bmatrix} 1 & 0 \end{bmatrix}$$

For the above linear state space model, the LQ control input that minimizes the quadratic form of the state variables and control inputs is calculated as follows:

$$J(u) = \int_0^\infty [x^T(t)Qx(t) + u^T(t)Ru(t)]d(t), Q = Q^T > 0, R = R^T > 0 \qquad (39)$$

$$u_0(t) = -R^{-1}B^T K x(t) \qquad (40)$$

Where, K is the solution of the following discrete Riccati matrix equation.

$$A^T SA - S - (A^T SB + N)(B^T SB + R)^{-1}(B^T SA + N^T) + Q = 0$$
$$K = (B^T SB + R)^{-1}(B^T SA + N^T) \qquad (41)$$

Thus, the actual control law is determined as follows to compensate the extended disturbance component.

$$u = u_0 - \frac{\hat{x}_4}{b} \qquad (42)$$

Results and Discussion

The simulation is performed using Matlab Simulink function.

The parameters of the control plant used in the simulation determined by the following values:

Table 1. Parameters of the dynamic model.

Parameter	Meaning	Value
ke	motor parameter	1
kr	motor parameter	0.1
kR	motor parameter	1

Copyright © 2025, Authors retain copyright. Licensed under the Creative Commons Attribution 4.0 International License (CC BY 4.0), which permits unrestricted use, distribution, and reproduction in any medium, provided the original work is properly cited. https://creativecommons.org/licenses/by/4.0/ (CC BY 4.0 deed)

WAR Journal of Multidisciplinary Bulletin
(WARJMB)
ISSN (Online): 1595-6709
ISSN (Print): 1595-6636
Received: 02-10-2025 Revised: 26-10-2025 Accepted: 05-11-2025 Published: 18-11-2025

r, m	radius of driving wheel	0.1
J, kgm2	driving wheel moment of inertia	0.005
m, kg	driving wheel mass	1
M, kg	vehicle weight	20

First, the proportional feedback control system according to Eq. (25) is simulated. Figure 3 illustrates the step response curves of the feedback system with various proportional feedback gains.

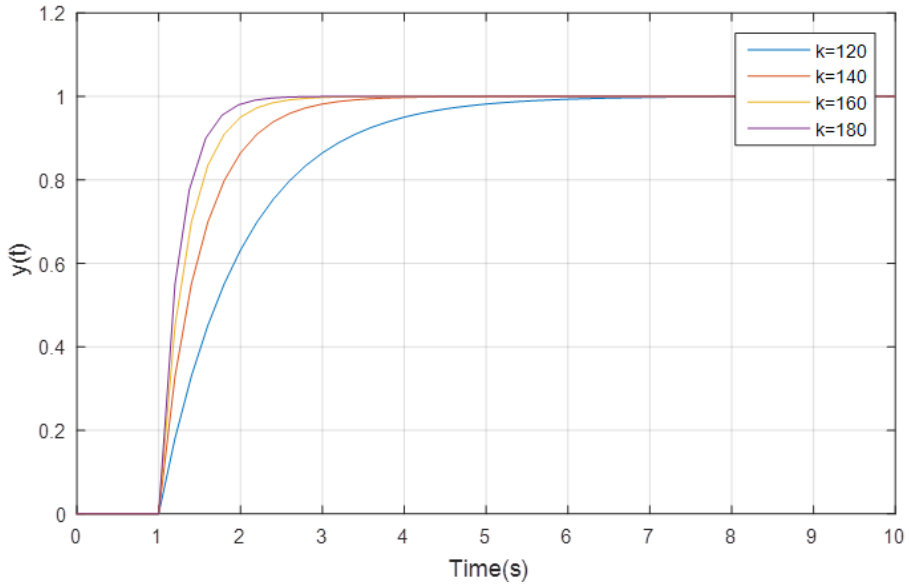

Figure 3. Step response of proportional feedback control system in speed loop.

As shown in the Figure 3, the higher the feedback coefficient, the faster the control response. However, the larger the feedback coefficient, the higher the manipulated variable increases, therefore it is chosen to be k=160 so that the control voltage of the motor not to be saturated. Then, we simulate the state estimation performance of an ESO with variable poles and compare the transient performance between different observers. The nonlinear function of Eq. (37) is chosen such that the pole decreases exponentially with increasing error.

$$\varphi_i(e_1(k)) = sign(e_1(k))\exp(-\alpha_i|e_1(k)| - \beta) + p_{\min} \quad (43)$$

The main purpose of the ESO is to estimate the unknown equivalent disturbance, so we simulate the state estimation process when the disturbance signal is applied. The disturbance was used as a step signal with amplitude 1.

The variation of observer poles following error and the variation of observer gain are shown in Figures 4 and 5, respectively. As shown in the Figures 4-5, the change of the pole is about 0.002 and the change of the gain is about 0.6.

Copyright © 2025, Authors retain copyright. Licensed under the Creative Commons Attribution 4.0 International License (CC BY 4.0), which permits unrestricted use, distribution, and reproduction in any medium, provided the original work is properly cited. https://creativecommons.org/licenses/by/4.0/ (CC BY 4.0 deed)

WAR Journal of Multidisciplinary Bulletin
(WARJMB)
ISSN (Online): 1595-6709
ISSN (Print): 1595-6636
Received: 02-10-2025 Revised: 26-10-2025 Accepted: 05-11-2025 Published: 18-11-2025

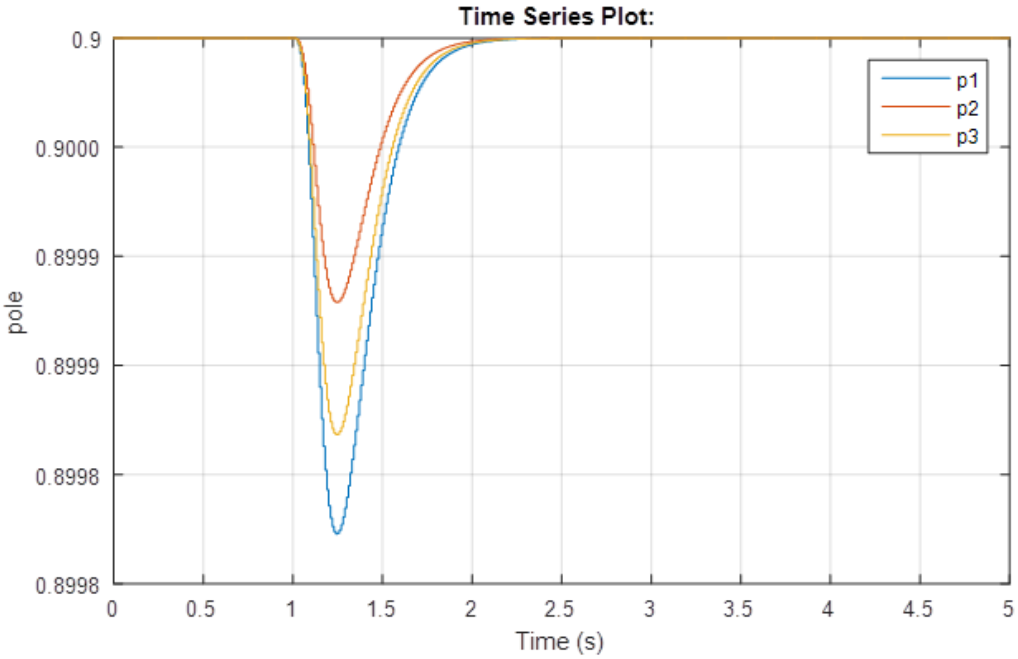

Figure 4. Curve of variation of the pole following error.

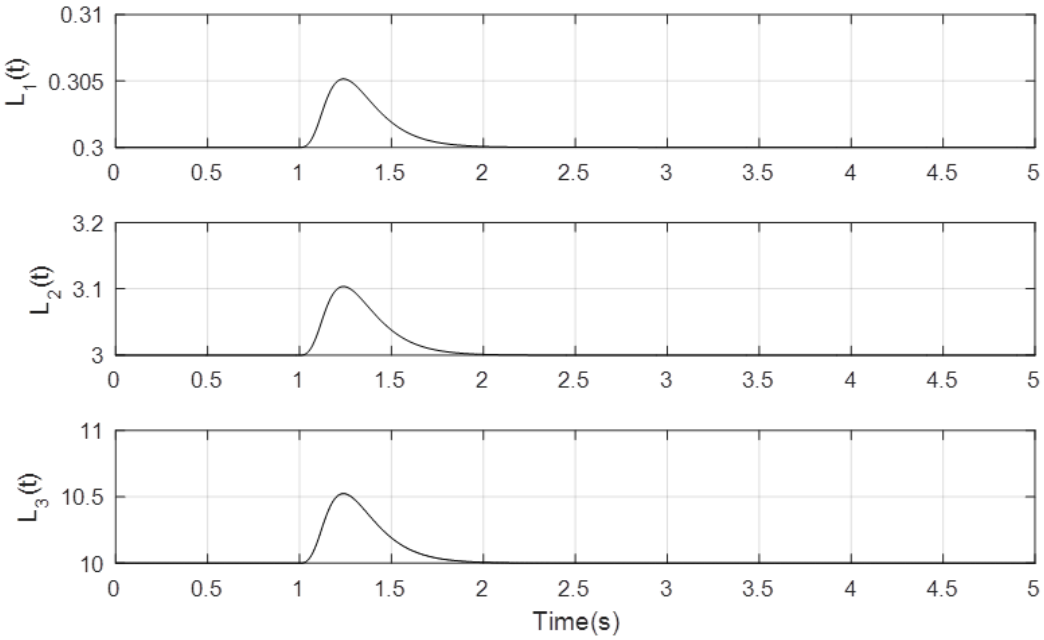

Figure 5. Variation curve of the ESO gain with error.

We compare the performance of the ESO with fixed poles and with variable poles.

Copyright © 2025, Authors retain copyright. Licensed under the Creative Commons Attribution 4.0 International License (CC BY 4.0), which permits unrestricted use, distribution, and reproduction in any medium, provided the original work is properly cited. https://creativecommons.org/licenses/by/4.0/ (CC BY 4.0 deed)

WAR Journal of Multidisciplinary Bulletin
(WARJMB)
ISSN (Online): 1595-6709
ISSN (Print): 1595-6636
Received: 02-10-2025 Revised: 26-10-2025 Accepted: 05-11-2025 Published: 18-11-2025

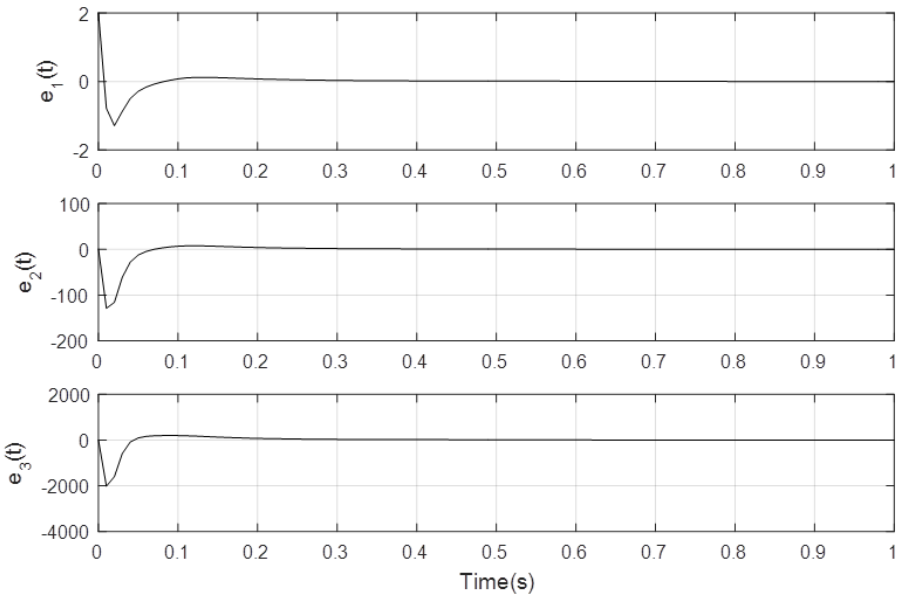

Figure 6. State estimation curve of VPPESO.

As shown in the Figure 6, the state estimation error of the state observer converges to zero within 0.1s even in the presence of disturbances. Figure 7 shows the state estimation results for the case of fixing the state observer poles to [0.52, 0.53, 0.51]. Compared with the estimation process in Figure 6, we can see that the estimation error convergence process of the state observer with variable poles is much faster. Furthermore, the use of a VPPESO can reduce the saturation of the feedback control by suppressing the overshoot in the state estimation process.

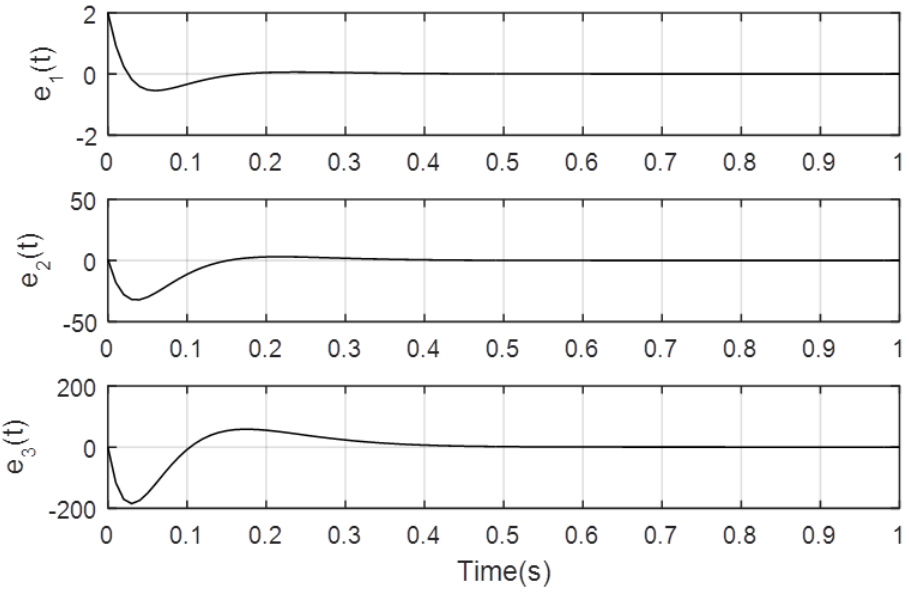

Figure 7. State estimation error of extended state observer with fixed poles

A performance comparison between VGESO in [16] and the proposed VPPESO is carriedout. Figure 10 shows the state errors according to the observers.

Copyright © 2025, Authors retain copyright. Licensed under the Creative Commons Attribution 4.0 International License (CC BY 4.0), which permits unrestricted use, distribution, and reproduction in any medium, provided the original work is properly cited. https://creativecommons.org/licenses/by/4.0/ (CC BY 4.0 deed)

WAR Journal of Multidisciplinary Bulletin
(WARJMB)
ISSN (Online): 1595-6709
ISSN (Print): 1595-6636
Received: 02-10-2025 Revised: 26-10-2025 Accepted: 05-11-2025 Published: 18-11-2025

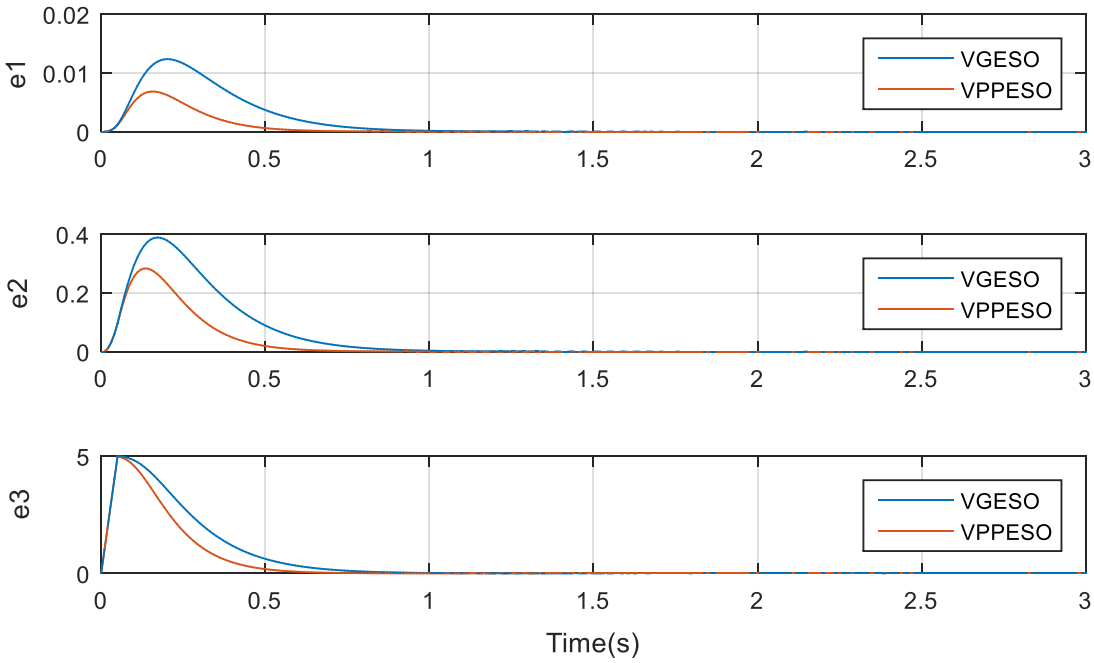

Figure 8. Error results of VPPESO and VGESO.

As shown in Figure 8, it can be seen that the transient performance of the proposed VPPESO is much better than that of VGESO.

We compare with performance between different ESOs by using RMS index. Table 2 shows the RMS index of the state estimation errors between different observers.

Table 2. RMS of the state estimation error in different ESOs

RMS	$x_1(t)$	$x_2(t)$	$x_3(t)$
VPPESO	0.0007	0.0386	0.8885
VGESO [16]	0.0016	0.0655	1.0617

Table 2 presents that the proposed VPPESO has much smaller state estimation error than VGESO.

Next, the control response of the ADRC system is simulated. In the linear quadratic optimal controller design, when Q and R are given by diag (10, 2) and 1, respectively, the state feedback coefficient is obtained as follows:

K=[1.6188, 0.7541]

Copyright © 2025, Authors retain copyright. Licensed under the Creative Commons Attribution 4.0 International License (CC BY 4.0), which permits unrestricted use, distribution, and reproduction in any medium, provided the original work is properly cited. https://creativecommons.org/licenses/by/4.0/ (CC BY 4.0 deed)

WAR Journal of Multidisciplinary Bulletin
(WARJMB)
ISSN (Online): 1595-6709
ISSN (Print): 1595-6636
Received: 02-10-2025 Revised: 26-10-2025 Accepted: 05-11-2025 Published: 18-11-2025

Figure 9 shows the step response of the ADRC system.

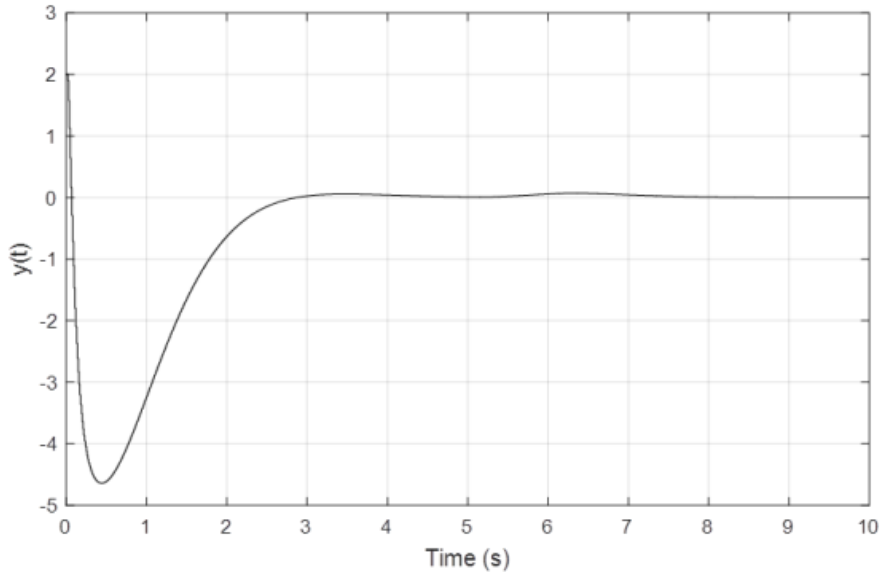

Figure 9. Step response of ADRC system.

Figure 10 shows the step response curves with the parameters of the PI controller. Then, step disturbance of amplitude 1 is applied at 5s.

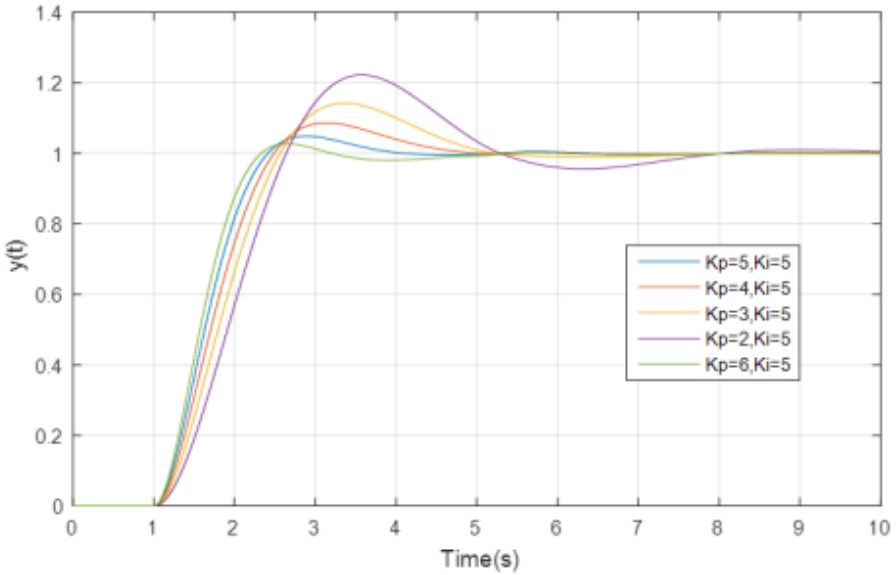

Figure 10. Step response of ADRC system including PI controller.

Then, we compare the control performance of the proposed control system and previous work [16]. Figure 11 shows the step response curves of the two control systems.

Copyright © 2025, Authors retain copyright. Licensed under the Creative Commons Attribution 4.0 International License (CC BY 4.0), which permits unrestricted use, distribution, and reproduction in any medium, provided the original work is properly cited. https://creativecommons.org/licenses/by/4.0/ (CC BY 4.0 deed)

WAR Journal of Multidisciplinary Bulletin
(WARJMB)
ISSN (Online): 1595-6709
ISSN (Print): 1595-6636
Received: 02-10-2025 Revised: 26-10-2025 Accepted: 05-11-2025 Published: 18-11-2025

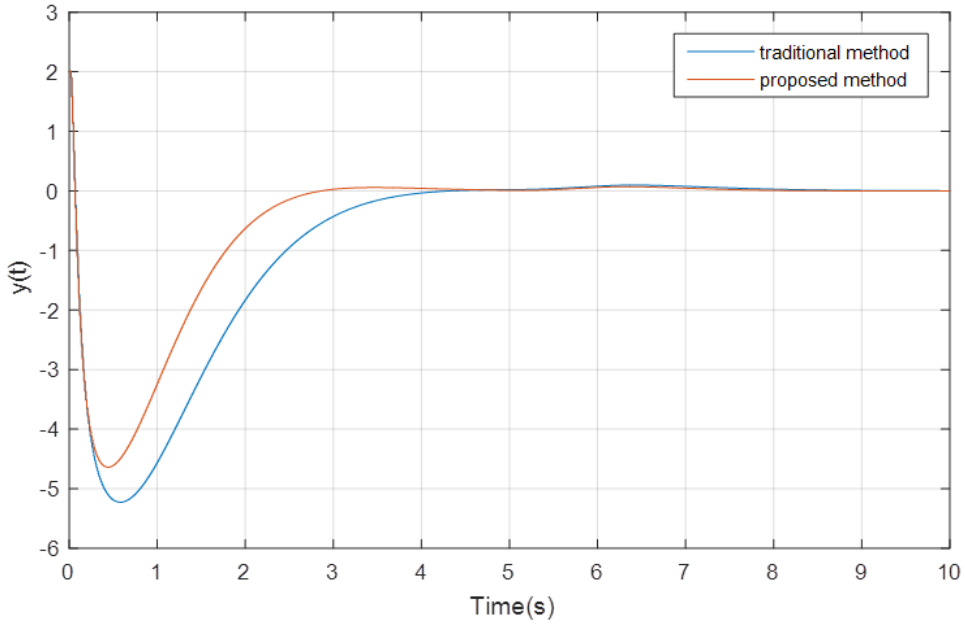

Figure 11. Comparison with the control approach of [16].

As shown in Figure 11, the response of the control system proposed in this paper is about 0.8 s short in settling time. Next, the control simulation of the path tracking system including the external control loop is simulated.

The control parameters for the outer loop control are given as follows:
k1=k2=0.5

Figure 12 shows the tracking process for the target trajectory.

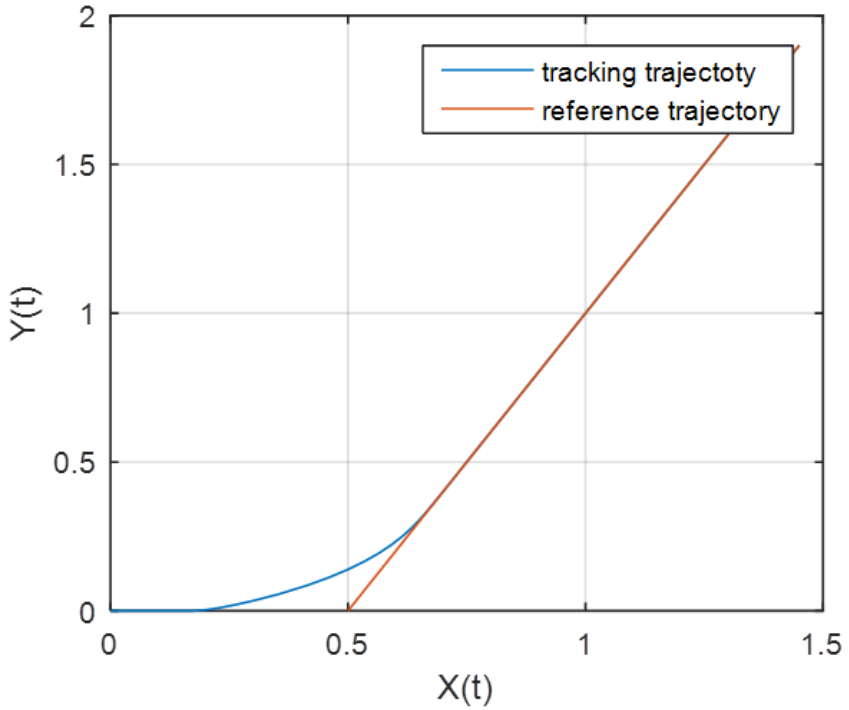

Figure 12. Tracking process of target trajectory.

Copyright © 2025, Authors retain copyright. Licensed under the Creative Commons Attribution 4.0 International License (CC BY 4.0), which permits unrestricted use, distribution, and reproduction in any medium, provided the original work is properly cited. https://creativecommons.org/licenses/by/4.0/ (CC BY 4.0 deed)

WAR Journal of Multidisciplinary Bulletin
(WARJMB)
ISSN (Online): 1595-6709
ISSN (Print): 1595-6636
Received: 02-10-2025 Revised: 26-10-2025 Accepted: 05-11-2025 Published: 18-11-2025

As shown in Figure 12, it can be seen that AGV tracks the target trajectory accurately from the initial starting point.

Conclusions

In this paper, a discrete disturbance rejection control system based on a novel VPPESO is proposed for tracking control of AGVs. First, an external control loop of speed and attitude for path tracking is designed and a mathematical model of the inner loop control plant is derived. Then, we estimate the disturbance using a discrete extended state observer and design an ADRC. The proposed new approach improves the estimation performance of the extended disturbance by varying the feedback coefficient of the extended state observer according to the magnitude of the error. Furthermore, the control method proposed in this paper can be applied to different unmanned robots working in hostile environments such as space exploration or marine exploration. The paper has a disadvantage that the dynamics of the motor is not considered. In the future, the author will further study the design problem of the ESO and ADRC of the third-order system with motor dynamics.

Acknowledgments

This work was supported by Kim Chaek University of Technology, Democratic People's Republic of Korea. The supports are gratefully acknowledged.

References

1. Zou Y., Y. Xing, M. et al. Image Blur Classification and Unintentional Blur Removal[J] // IEEE ACCESS. 2019. Vol 7. P. 215-224.
2. Aguilar-Gonzalez, A., Lozoya, C., Orona, L., Romo, S., Roman-Flores, A. Campus kart: An automated guided vehicle to teach using a multidisciplinary approach// IEEE. Revi .Iberoam .De .Tecn. Del .Apr. 2017. Vol 12. P.199-207.
3. Sabattini, L., Fuerstenberg, K., Secchi, and C., et al. The PAN-robots project: Advanced automated guided vehicle systems for industrial logistics// IEEE. Robot. Autom. Mag. 2018. Vol 25(1). P. 55-64.
4. Ba£ík, J., urovský, F., Biro², M., Kyslan, K., Perduková, D., Padmanaban, S. Pathnder development of automated guided vehicle for hospital logistics// IEEE Access. 2017. Vol 5. P. 26892-26900.
5. Xie, L., Stol, K., Xu, W. Energy-optimal motion trajectory of an omnidirectional mechanism-wheeled robot via polynomial functions// Robotica. 2020. Vol 38(8). P. 1400-1414.
6. Wang, C., Liu, X., Yang, X., Hu, F., Jiang, A. Yang, C. Trajectory tracking of an omni-directional wheeled mobile robot using a model predictive control strategy// Appl. Sci. 2018. Vol 8(2).
7. Sun, Z., Hu, S., Xie, H., Li, H., Zheng, J., Chen, B. Fuzzy adaptive recursive terminal sliding mode control for an agricultural omnidirectional mobile robot// Comput. Elect. Eng, Art. 2023. Vol 105(108529).
8. Zou, Y., Guo, N., Zhang, X. An integrated control strategy of path following and lateral motion stabilization for autonomous distributed drive electric vehicles// Proc. Inst. Mech. Eng. D J. Automob. Eng. 2021. Vol 235(4). P. 1164-1179.
9. Hameerlain, F., Floquet, T., Perruquetti, W. Experimental tests of a sliding mode controller for trajectory tracking of a car-like mobile robot// Robotica. 2014. Vol 32. P. 63-76.
10. Tang, Z., Xu, X., Wang, F., et al. Coordinated control for path following of two-wheel

Copyright © 2025, Authors retain copyright. Licensed under the Creative Commons Attribution 4.0 International License (CC BY 4.0), which permits unrestricted use, distribution, and reproduction in any medium, provided the original work is properly cited. https://creativecommons.org/licenses/by/4.0/ (CC BY 4.0 deed)

WAR Journal of Multidisciplinary Bulletin
(WARJMB)
ISSN (Online): 1595-6709
ISSN (Print): 1595-6636
Received: 02-10-2025 Revised: 26-10-2025 Accepted: 05-11-2025 Published: 18-11-2025

independently actuated autonomous ground vehicle// IET Intel. Transport Syst. 2019. Vol 13. P. 628-635.

11. Cui, Q., Ding, R., Wei, C., Zhou, B. Path-tracking and lateral stabilization for autonomous vehicles by using the steering angle envelope// Veh. Syst. Dyn. 2020. Vol 59(11). P.1672-1696.
12. Ma, X., Guo, Y., Chen, L. Active disturbance rejection control for electric power steering system with assist motor variable mode, J. Franklin Inst. 2018. Vol 355(3). P.1139-1155.
13. Lamraoui, H. C., Qidan, Z., Bouzid, Y. Improved active disturbance rejecter control for trajectory tracking of unmanned surface vessel// Marine Systems and Ocean Technology. 2022. Vol 17. P. 18-26.
14. Fareh, R., Al-Shabi, M., Bettayeb, M., Ghommam, J. Robust active disturbance rejection control for flexible link manipulator// Robotica. 2019. P. 1-18.
15. Guo, B. Z., Wu, Z. H. Active disturbance rejection control approach to output-feedback stabilization of lower triangular nonlinear systems with stochastic uncertainty// International journal of robust and nonlinear control.2017. Vol 27. P. 2773-2797.
16. Li, J., Xia, Y., Qi, X., Wan, H. On convergence of the discrete-time nonlinear extended state observer//J. Franklin Inst. 2018. Vol 355(1). P. 501-519.
17. Li, S., Zhang, J., Gu, S. Discrete time trajectory tracking control for four-mecanum-wheeled mobile vehicle: An variable gain ADRC method// IEEE Robotics. 2024. Vol 9. P. 7771-7778.

Copyright © 2025, Authors retain copyright. Licensed under the Creative Commons Attribution 4.0 International License (CC BY 4.0), which permits unrestricted use, distribution, and reproduction in any medium, provided the original work is properly cited. https://creativecommons.org/licenses/by/4.0/ (CC BY 4.0 deed)